PERGAMON

International Journal of Heat and Mass Transfer 43 (2000) 101–111

International Journal of HEAT and MASS TRANSFER

www.elsevier.com/locate/ijhmt

Plasma flow over an array of particles

Alok Verma, Milind A. Jog*

Department of Mechanical, Industrial and Nuclear Engineering, University of Cincinnati, PO Box 210072, Cincinnati, OH 45221-0072, USA

Received 3 September 1998; received in revised form 26 March 1999

Abstract

This paper presents an analysis of heat and momentum transport to an array of particles from a flow of a collision-dominated weakly ionized gas consisting of electrons, ions, and neutrals. The particle longitudinal and lateral spacing is varied independently to study the effect of particle spacing on the flow and heat transport. The conservation equations for mass, momentum, and energy for the neutrals and those for ions and electrons are solved simultaneously with the Poisson's equation for the self-consistent electric field. Solutions are obtained using a finite volume method and the formulation is based on a cylindrical-cell model. An orthogonal adaptive grid is generated to body-fit the particle surfaces as well as the cylindrical outer boundary of the cell envelop. The flow field and the temperature distributions are obtained in the plasma and the overall Nusselt number and the drag force acting on each particle are determined. Results indicate that the flow and transport around a given particle is significantly influenced by the presence of the neighboring particles. An increase in the lateral spacing between particles results in a decrease in the Nusselt number as well as the drag coefficient, whereas increasing longitudinal particle spacing leads to an increase in both the Nusselt number and the drag coefficient. The effect of side particles becomes negligible for lateral spacings greater than about five diameters. However, the influence of upstream particles remains significant even at longitudinal particle spacing of five diameters. Correlations that incorporate the effects due to neighboring particles have been proposed for the drag coefficient and the Nusselt number of an interior particle in the array.

1. Introduction

Plasma flow over a large number of particles is encountered in induction plasma spraying process. In this process, ceramic/metallic particles are introduced in a flow of thermal plasma. The heat transfer from the plasma to the particles results in heating and melting of the particles. The molten particles then impinge on a substrate to be coated. Subsequent spreading and solidification forms a thin layer on the substrate. As particle velocity and temperature affects the quality of the coating [1], it is important to predict and control the particle momentum and heat transport. Pfender and co-workers [2,3] and Boulos and co-workers [4,5] provide extensive reviews of the studies on the momentum and heat transfer to particles from plasma flow. Most of the work has been carried out for flow over an isolated particle. Young and Pfender [6] provide a comparison of available Nusselt number correlations for plasma flow over an isolated sphere.

Simulations of particle/plasma flow and heat transfer in induction plasma torch [7,8] have typically employed the particle-source-in-cell method [9]. In this method, for each time step, the continuity, momentum conservation, and the energy conservation equations

* Corresponding author. Tel.: +1-513-556-1675; fax: +1-513-556-3390.

E-mail address: milind.jog@uc.edu (M.A. Jog)

0017-9310/00/$ - see front matter
PII: S0017-9310(99)00116-7

Nomenclature

$2a$	lateral spacing between particles
C_D	drag coefficient
d	particle diameter
D	diffusivity
e	magnitude of charge on a single electron
h_ξ, h_η, h_ϕ	metric coefficients in the curvilinear coordinates (ξ, η, ϕ)
k	thermal conductivity
k_B	Boltzmann constant
l	longitudinal spacing between particles
N	number density
Nu	Nusselt number
p	pressure
P	rate of production of charged species
Pe	Peclet number ($RePr$)
Pr	Prandtl number
r_p	particle radius
r, z, ϕ	coordinates in the physical domain
R	rate of recombination of charged species
Re	Reynolds number based on particle diameter
Sc	Schmidt number
T	temperature
u	velocity
U_∞	free stream velocity
V	electric potential

Greek symbols

β	D_i/D_e
ε	ratio of Debye length to diameter (λ_D/d)
Γ	flux of charged species
λ_m	mean free path
λ_D	Debye length
μ	mobility
ν	kinematic viscosity
ρ	density
ψ	stream function
ω	vorticity
ξ, η, ϕ	coordinates in the computational domain

Subscripts/superscripts

av	average value
e	electron
i	ion
n	neutral
s	isolated sphere
*	dimensionless quantities

for the continuous phase are solved first. The drag force and heat transfer to the particles are considered as momentum/energy source terms in the corresponding equations for the continuous phase. The source terms for a computational cell are determined by summing the contribution of individual particles in that cell by using drag force and Nusselt number correlations for an isolated particle. The particle trajectories are then determined based on the calculated flow field. In plasma spraying process, due to the injection of a large number of particles into the plasma flow, the flow field and heat transfer around a given particle gets significantly affected by the proximity of neighboring particles. Therefore, the appropriate Nusselt number and drag coefficients for closely spaced particles are likely to be considerably different from that for an isolated sphere, and are needed to incorporate the effects due to inter-particle interactions in induction plasma spray simulations. Such effects due to neighboring particles have not been addressed before in plasma spraying. However, gas flow over a multiparticle configurations has received considerable attention in the context of fuel sprays in combustion systems. These studies are discussed in detail in a monograph by Sadhal et al. [10] and a recent review by Ayyaswamy [11]. Many of the studies of gas flow over multiple particles utilize a cylindrical cell model developed by Tal et al. [12,13] to describe the hydrodynamics of particle assemblages. In this model, an array of uniformly spaced spheres is considered as shown in Fig. 1. Due to the symmetry and periodic nature of the array, no heat and momentum transfer is assumed to occur at lateral equidistant planes between the columns of spheres. This reduces the analysis to a multitude of spheres in tandem in a square stream tube. The three-dimensional flow situation in the square stream tube is then simplified to an axisymmetric analysis by replacing it with a cylindrical duct. Although, in general, particle spray problem may be non-axisymmetric, invoking axisymmetry can indeed serve as a useful approximation for a reasonably symmetric distribution of neighbors around the flow axis (for a detailed discussion, see Ayyaswamy and co-workers [14,15]). Flow over an array of spheres with equal stream-wise and lateral spacing at a Reynolds number of 100 was considered by Tal et al. [12]. They showed a decrease in drag force and Nusselt number for the downstream spheres compared to those for the leading sphere. An important contribution was the identification of periodicity that was seen to evolve in the flow and temperature field after the first sphere. They used a non-uniform cylindrical

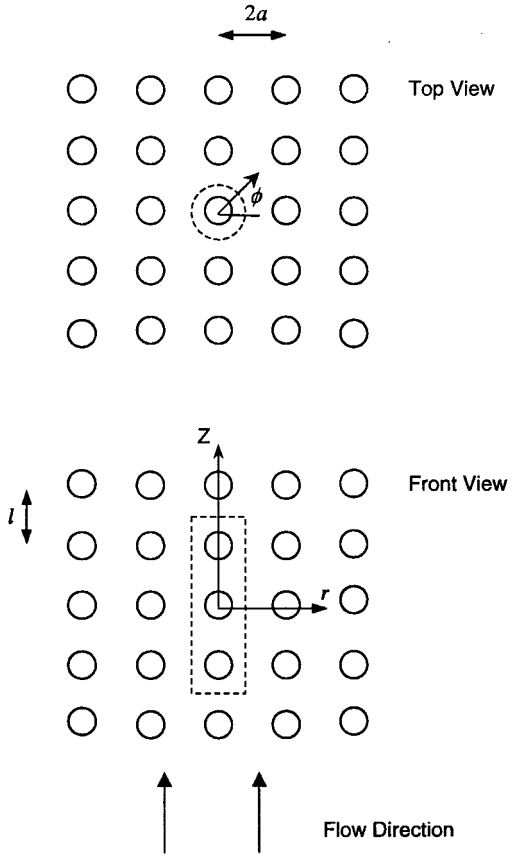

Fig. 1. Schematic of the cylindrical-cell model.

grid that does not provide the same numerical accuracy of a fine uniform mesh around the particle surface. The grid used in the numerical solution was later improved by Chen and Tong [16] as an elliptical body-fitted grid in their study of vaporizing liquid droplet array. Due to the accuracy and flexibility of the grid desired near the particle surfaces, Tsai and Sterling [17] employed an embedded grid to study heat and momentum transfer to a linear array of spheres. The embedded grid was created by generating a spherical-algebraic grid close to the sphere surface and a numerical, curvilinear body-fitted grid in the remaining flow region. This feature allows for accurate resolution of steep velocity and temperature gradients in the vicinity of the sphere surface. Their results indicate that drag coefficient and Nusselt number for the first sphere are higher than those for the downstream spheres. However the values of C_D and Nu for the second and the third sphere are nearly equal. All of these studies show that when the streamwise inter-particle spacings are equal, the drag coefficient and the Nusselt number for the second and the follower spheres are very close, and as such the results for the second sphere can reasonably mimic the behavior of any interior sphere of the array. Finite element methods have also been used to study the flow and heat transfer for drops/spheres in tandem [18,19].

We note that gas ionization introduces further complexities in flow and transport. Chung et al. [20] provide a review of the studies on the interaction between a spherical body and an ionized gas. Once the particles are introduced in an ionized gas, owing to the large differences in mobilities of ions and electrons, initially more electrons impact on the surface of the particles than ions. The particles become negatively charged with respect to the main body of the plasma such that the current of ions and electrons towards a particle are equal. Under this condition, the electric potential at the particle surface with respect to the plasma is known as the floating potential. A charge sheath, with high gradients of ion and electron number densities and the electric potential, is present close to particle surface whereas the main body of the plasma is charge neutral [21,22]. The transport of electrons and ions and their contributions to the heat transport need to be taken into account. For induction spraying applications, the plasma temperatures are typically lower than 10,000 K and the limit $\lambda_m < \lambda_D < r_p$ is satisfied, where λ_m is the mean free path, λ_D is the Debye length, and r_p is the particle radius. Under this limit, the heat transfer from a stationary plasma to solid surfaces has been modeled by Sripada et al. [23] and Jog et al. [24]. Recently we have analyzed plasma flow over a spherical particle under this condition [25]. Our results indicate that accounting for energy transport to the sphere surface by conduction from charged species and their recombination is necessary to accurately determine the particle heat transport.

In this paper, we have analyzed the flow of a weakly ionized gas over an array of particles and have provided correlations for drag force and Nusselt number that incorporate the effects of inter particle interactions. Considering a symmetric distribution of particles in an array, a typical array cell is analyzed. The effect of inter-particle interaction on the heat and momentum transport has been studied by independently varying the lateral and longitudinal spacing in the particle array. The grid has been obtained by incorporating recent developments in generation of *orthogonal* body-fitted grids [26]. An orthogonal grid results in simpler forms of the transformed equations by eliminating the cross derivative terms and it provides accurate representation of the boundary conditions with comparably lower discretization errors. Additionally, boundary point distribution control has been incorporated to aid the future extension of the work to non-spherical particle shapes.

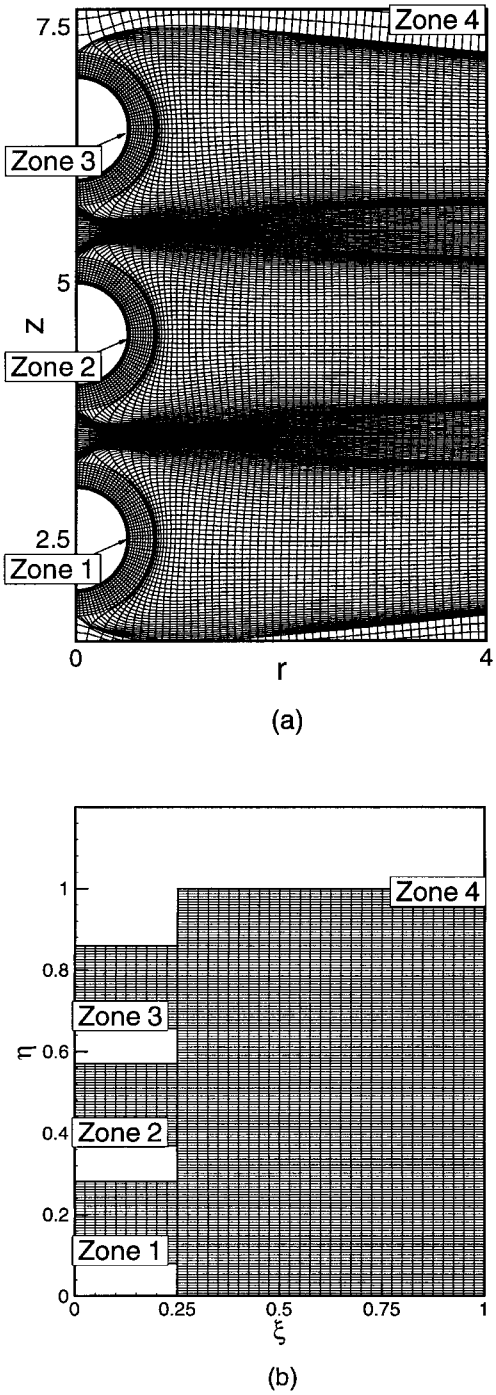

Fig. 2. (a) Physical domain for the three-sphere cell configuration and (b) computational domain.

2. Problem formulation

Consider an array of spherical particles of radius r with lateral spacing $2a$ and stream-wise separation l as shown in Fig. 1. We employ the cylindrical cell model. The flow around a particle in a cell is taken to by axisymmetric. As the particle surfaces and the cylindrical cell boundary are geometrically dissimilar, an orthogonal curvilinear grid is obtained that conforms to the particle surfaces as well as cell boundary as described below.

2.1. Grid generation

Fig. 2(a) shows a symmetrical half view of the physical domain. The corresponding computational domain is shown in Fig. 2(b). The physical domain is made up of four zones: three identical zones (1–3) and zone 4. Zones 1–3 are constructed by algebraically generating a spherical grid around each of the half circles representing the spherical particles. These zones (1–3) are incorporated to eliminate the intrinsic problem of non-orthogonality at the front stagnation and rear ends where the half circles meet the axis of symmetry. This ensures the accurate evaluation of the local transport parameters. These zones are coupled with the numerically generated orthogonal curvilinear grid in zone 4. Following a procedure recently outlined by Eca [26], the *orthogonal* curvilinear grid in zone 4 is obtained from solution of the following coupled, non-linear partial differential equations:

$$\left.\begin{aligned}\frac{\partial}{\partial\xi}\left(f\frac{\partial r}{\partial\xi}\right)+\frac{\partial}{\partial\eta}\left(f\frac{\partial r}{\partial\eta}\right)=0\\ \frac{\partial}{\partial\xi}\left(f\frac{\partial z}{\partial\xi}\right)+\frac{\partial}{\partial\eta}\left(f\frac{\partial z}{\partial\eta}\right)=0\end{aligned}\right\}. \tag{1}$$

Here f represents the distortion function and is defined as

$$f=\sqrt{\left(\frac{\partial r}{\partial\eta}\right)^2+\left(\frac{\partial z}{\partial\eta}\right)^2}\Bigg/\sqrt{\left(\frac{\partial r}{\partial\xi}\right)^2+\left(\frac{\partial z}{\partial\xi}\right)^2}. \tag{2}$$

The equation set (1) is discretized by applying the 'control volume' approach and using second order accurate central differencing for the first derivatives of the grid coordinates. Dirichlet boundary conditions are specified at all boundaries. The distortion function, f, at the four boundaries of the control volume is determined from the definition Eq. (2). The distortion function value is updated at the end of each inner cycle. Dual criteria are used for the convergence by monitoring the relative difference in distortion function, $\zeta=\max((f^n-f^{n-1})/f^n)$, as well as maximum deviation from orthogonality $\mathrm{MDO}=\max(90^\circ-\theta_{i,j})$ where $\theta_{i,j}$ is the angle between ξ and η grid lines at a grid location (i, j) and is given by

$$\theta_{i,j} = \cos^{-1}\left[\left(\frac{\partial r}{\partial \xi}\frac{\partial r}{\partial \eta}+\frac{\partial z}{\partial \xi}\frac{\partial z}{\partial \eta}\right)\Bigg/\left(\left(\left(\frac{\partial r}{\partial \eta}\right)^2+\left(\frac{\partial z}{\partial \eta}\right)^2\right)\left(\left(\frac{\partial r}{\partial \xi}\right)^2+\left(\frac{\partial z}{\partial \xi}\right)^2\right)\right)^{1/2}\right].$$

Grid solution is considered to converge when $\zeta \leq 10^{-4}$ and MDO $< 0.1^0$.

2.2. Governing equations and boundary conditions

We consider a flow of a weakly ionized gas consisting of electrons, ions, and neutrals. The far field pressure is atmospheric and the flow Reynolds number based on the particle diameter is in the intermediate regime ($Re \sim 20$–100). Good collision coupling exists between heavy species (ions and neutrals) and their temperatures are considered equal at any given location [4]. Steady, laminar flow has been assumed with constant thermo-physical properties. Experimental studies have shown that the particle temperature remains close to its melting temperature for most of the particle residence time in plasma spraying process [1,27]. Therefore, surface temperatures of all particles in the array are considered equal to the melting temperature in this analysis. The background gas Argon is assumed to be optically thin at the operating atmospheric pressure. Bourdin et al. [28], have shown that the heat transport to a stationary particle by radiation is negligible compared to that by conduction for far-field plasma temperatures greater than 4000 K. For moving particles, the convective heat transfer from plasma is much greater than pure conduction. Therefore, radiation is neglected compared to convection. The degree of ionization is small such that the overall velocity field can be determined by the solution of the continuity and the momentum conservation equation for the neutral gas [20]. The conservation equations for the charged particle density, electron energy with the Poisson's equation for the self-consistent electric field describe the behavior of the electrons and ions. The governing equations are rendered dimensionless using the following non-dimensional parameters: $r^* = r/d$, $u^* = u/U_\infty$, $p^* = p/\rho U_\infty^2$, $\nabla^* = d\nabla$, $V^* = eV/(k_B T_\infty)$, $N^*_{e,i} = N_{e,i}/N_o$, $T^* = T/T_\infty$, and $\Gamma^*_{e,i} = ed/(\mu_{e,i} N_o k_B T_\infty)\Gamma_{e,i}$. The Reynolds number $Re = U_\infty d/\nu$, the Prandtl number $Pr = \nu/\alpha$, the Schmidt number $Sc = \mu/\rho D$, $\beta = D_i/D_e$ and $\varepsilon = \lambda_D/d$. The Debye length is based on the undisturbed plasma properties $\lambda_D = [\varepsilon_0 k_B T_\infty/(e^2 N_o)]^{1/2}$, where ε_0 is the permittivity of free space. We assume that the Einstein relation $\mu/D = e/(k_B T)$ is satisfied by charged species. The governing equations can be written in terms of the above dimensionless parameters as:

$$\nabla^* \mathbf{u}^* = 0 \tag{3}$$

$$Re\mathbf{u}^*\nabla^*\mathbf{u}^* = -Re\nabla^* p^* + \nabla^{*2}\mathbf{u}^* \tag{4}$$

$$RePr\mathbf{u}^*\nabla^* T^*_n = \nabla^{*2} T^*_n \tag{5}$$

$$\beta ReSc_i \mathbf{u}^*\nabla^* N^*_e - \nabla^{*2}(N^*_e T^*_e) + \nabla^*(N^*_e \nabla^* V^*) = \frac{ed^2}{\mu_e K_B N_o T_\infty}(P - R) \tag{6}$$

$$ReSc_i \mathbf{u}^*\nabla^* N^*_i - \nabla^{*2}(N^*_i T^*_i) - \nabla^*(N^*_i \nabla^* V^*) = \frac{ed^2}{\mu_i k_B N_o T_\infty}(P - R) \tag{7}$$

$$\beta ReSc_i \mathbf{u}^*\nabla^*\left(\frac{3}{2}N^*_e T^*_e\right) + \nabla^*\left(\frac{5}{2}\Gamma^*_e T^*_e\right) = \frac{k_e e}{\mu_e k_B^2 N_o T_\infty}\nabla^{*2} T^*_e + \Gamma^*_e \nabla^* V^* \tag{8}$$

$$\varepsilon^2 \nabla^{*2} V = N^*_e - N^*_i. \tag{9}$$

The electron and ion fluxes are given by

$$\Gamma^*_e = -\nabla(N^*_e T^*_e) + N^*_e \nabla V^* \tag{10}$$

$$\Gamma^*_i = -\nabla(N^*_i T^*_i) - N^*_i \nabla V^*. \tag{11}$$

The electron temperature is expected to be high in the most of the domain and the thermal ionization and three body recombination will be the predominant mechanisms of the production and recombination of charged particles. The net production by thermal ionization and three body recombination is given by the Saha equations as [29]

$$P - R = \gamma N_e\left[\frac{2g_i N_n}{g_n}\left(\frac{2\pi m_e k T_e}{h^2}\right)^{3/2} \times \exp\left(-\frac{eV_i}{kT_e}\right) - N_e N_i\right] \tag{12}$$

where $\gamma = 1.09 \times 10^{-20} T_e^{-9/2}$ m^6/s [30].

The governing equations are subject the following boundary conditions: At the inlet, the condition of uniform inlet velocity, pressure, number densities, and free stream temperatures are imposed at the inflow

boundary. Incoming plasma is considered field free. $u^*_\eta = 1$, $u^*_\xi = 0$, $p^* = 1$, $T^*_{e,i,n} = 1$, $N^*_{e,i} = 1$, $V^* = 0$.

At the outlet, the outflow conditions are applied as $u^*_\xi = 0$, $V^* = 0$, $\partial/\partial\eta(u^*_\eta,\ T^*_{e,i,n},\ N^*_{e,i}) = 0$.

On the sphere surfaces no-slip and non-porous velocity boundary conditions are valid. The surface temperatures and number densities are specified. The particle surfaces are considered as a perfect sink for the electrons and ions, and as the surfaces are at the floating potential, the condition of equality of ion and electron fluxes is imposed. $u^*_\xi = u^*_\eta = 0$, $T^*_{e,i,n} = T^*_s$, $N^*_{e,i} = N^*_s$ and $\mu_e \Gamma^*_e = \mu_i \Gamma^*_i$. Along the center line the symmetry conditions are applied: $u^*_\xi = 0$, $\partial/\partial\eta(u^*_\eta,\ T^*_{e,i,n},\ N^*_{e,i},\ V^*) = 0$ in Zones 1–3; and $u^*_\eta = 0$, $\partial/\partial\xi(u^*_\xi,\ T^*_{e,i,n},\ N^*_{e,i},\ V^*) = 0$ in Zone 4.

On the cylindrical cell envelop $u^*_\xi = \partial/\partial\xi(u^*_\eta,\ T^*_{e,i,n},\ N^*_{e,i},\ V^*) = 0$.

The continuity, the momentum conservation, and the energy conservation equations for the neutrals (Eqs. (3)–(5)) are solved in the entire computational domain using a stream function–vorticity formulation. In a region of several Debye lengths adjacent to the sphere surface, the charged particle densities are expected to be small and the gradients of electric potential and the number densities are expected to be large. This is known as the electric sheath region. The complete set of governing equations for the charged species (Eqs. (6)–(9)) needs to be solved in this region. Except for this thin electric sheath, in the majority of the flow field the charged particle densities are expected to be high and nearly equal, and the gradients of temperature and the electric field are expected to be small. This is referred to as the quasi-neutral region. We can simplify a part of the above set of equations in that region. As the charged particle densities are expected to be large and nearly equal, and the electric field is small, the left-hand side of Eq. (9) becomes very small compared to the two terms on the right-hand side. Therefore, Eq. (9) simplifies to give the well-known quasi-neutral solution as $N^*_e = N^*_i \equiv N^*$. Using this result and multiplying Eq. (6) by μ_e and Eq. (7) by μ_i and subtracting we get

$$\nabla^*(N^*\nabla^* V^*) = \frac{\mu_e}{\mu_e + \mu_i}\nabla^{*2}(N^* T^*_e) - \frac{\mu_e}{\mu_e + \mu_i}\nabla^{*2}(N^* T^*_i). \tag{13}$$

In the quasi-neutral region, the right-hand side of Eqs. (6) and (7) show a balance between two very large numbers compared to the left-hand side. This is the balance of thermal ionization and recombination, $P \approx R$. Therefore in the quasi-neutral region

$$N^{*2} = \frac{2 g_i N_n}{g_n N_o^2}(2\pi m_e k T_\infty/h^2)^{3/2} T^{*3/2}_e \exp(-V^*_i/T^*_e). \tag{14}$$

Eqs. (13) and (14) are solved simultaneously with the electron energy equation (Eq. (8)) to get the common density, electric potential, and electron temperature variation in the quasi-neutral region. The solutions in the entire computational domain for the charged particle densities, temperatures, and the electric potential are obtained by matching the solutions in the quasi-neutral region to those in the sheath region by an iterative matching technique as described later.

3. Computational methodology

The governing equations and the boundary conditions are transformed in terms of the dimensionless stream function ψ (scaled with $U_\infty d^2$) and vorticity ω (scaled with U_∞/d). The governing equations are first written in the cylindrical–polar coordinates and then transformed to the orthogonal curvilinear coordinates, $(\xi,\ \eta,\ \phi)$. Note that due to the axially symmetric nature of the formulation $\partial/\partial\phi = 0$, $u_\phi = 0$, and $\omega_\xi = \omega_\eta = 0$. First, the flow field and the temperature distribution are obtained for the background gas. The governing equations are discretized by the control volume technique and the resulting algebraic equations are solved iteratively. A power law scheme, based on Patankar's generalized formulation [31], is employed to handle the convective-diffusive terms. The temperature field for neutrals is subsequently obtained by solving the energy equation (Eq. (7)). An under-relaxation factor of 0.6 was adequate for both the vorticity and energy equations. The convergence criterion (maximum absolute error in the dependent variables between two successive iterations) in all runs was set at 10^{-5}.

Next, the governing equations for the charged particle densities, electron temperature, and the electric potential are solved simultaneously. First guess is made for the charged particle densities and the electric field. Using these guess values electron temperature variation is obtained by solution of Eq. (8). Corresponding values for the common number density are calculated. Grid points are chosen where the number densities are $O(\varepsilon^{-2})$. The governing equations for the sheath are then solved toward the surface. These solutions in the sheath region provide the matching boundary conditions required to solve the governing equations in the quasi-neutral region. The electron temperature is recalculated and this iterative procedure is continued until convergence is obtained. Due to the

coupled and non-linear nature of the equations, under relaxation was used with relaxation coefficients between 0.8 and 1.0.

3.1. Physical quantities

From the velocity field the viscous stresses acting on the particles are obtained. The distribution of the non-dimensional pressure is determined along the particle surfaces by line integration of the momentum conservation equation. (For details see [32]). The total drag coefficient is given by $C_D = C_{DF} + C_{DP}$, where the friction drag coefficient is evaluated as

$$C_{DF} = \frac{16}{Re}\int_{surface} r^*\omega^*\frac{\partial z}{\partial \eta}\,d\eta \tag{15}$$

and the pressure drag coefficient is given by

$$C_{DP} = -\int_{surface} 8rp^*\frac{h_\xi^*}{h_\eta^*}\frac{\partial z}{\partial \xi}\,d\eta. \tag{16}$$

Here h_ξ, h_η, and h_ϕ are the metric coefficients defined as

$$h_\xi = \left[\left(\frac{\partial r}{\partial \xi}\right)^2 + \left(\frac{\partial z}{\partial \xi}\right)^2\right]^{-1/2}, \qquad h_\eta = \left[\left(\frac{\partial r}{\partial \eta}\right)^2 + \left(\frac{\partial z}{\partial \eta}\right)^2\right]^{-1/2}, \quad h_\phi = \frac{1}{r}. \tag{17}$$

Once the temperatures of the electrons, the ions and the neutrals are determined, the energy transferred to the particle surface can be calculated by accounting for all the modes of heat transport to the surface. The net heat transport is given by $q = q_r + q_e + q_i + q_n$. Here q_r is the energy deposited by recombination of the ions and electrons at the surface equivalent to the ionization potential. $q_r = e\Gamma_e V_i$. The electrons and ions also deposit their thermal energy by conduction.

$$q_e = -k_e h_\xi \frac{\partial T_e}{\partial \xi}, \quad q_i = -k_i h_\xi \frac{\partial T_i}{\partial \xi}.$$

The conduction of heat from the neutral gas is given by

$$q_n = -k_n h_\xi \frac{\partial T_n}{\partial \xi}.$$

The local Nusselt number is

$$Nu_{local} = \frac{qd}{(T_s - T_\infty)k_n}$$

and the overall Nusselt number is given by

$$Nu = 2\int_{surface} \frac{Nu_{local} r^*}{h_\eta^*}\,d\eta.$$

Table 1
Comparison of results for validation of the computational model

$Re = 100$, $Pr = 0.7$ $a/d = 2$	Sphere 1	Sphere 2	Sphere 3
C_D (present study)	0.994	0.421	0.71
Ramachandran et al. [19]	0.995	0.423	0.462
Nu (present study)	6.779	4.035	3.89
Ramachandran et al. [19]	6.852	4.027	3.92

4. Results and discussion

The results were obtained for inter-particle longitudinal and lateral spacing from 1.5 to 5 diameters. The background gas was considered argon at atmospheric pressure. The particle surface temperature was taken as melting temperature for alumina, a commonly used material for plasma spraying, $T = 2323$ K and $T_\infty = 8000$ K. Electrical and thermo-physical properties were obtained from Refs. [4] and [33]. Solutions were obtained with 101×301 grid points in zone 4 and 61×61 grid points each in zones 1–3. To ascertain grid independence, results for four test cases ($l/d = 2$, 4 and $Re = 20{,}100$, with $a/d = 2.5$) were obtained with doubling the grid point in both directions. The overall drag coefficient and Nusselt number changed by less than 1%. The numerical code was validated by

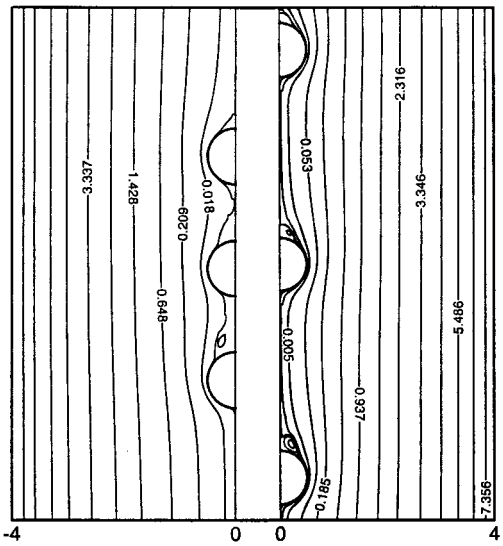

Fig. 3. Stream function plots for $l/d = 2$ and 4 at $Re = 50$ and $a/d = 4$.

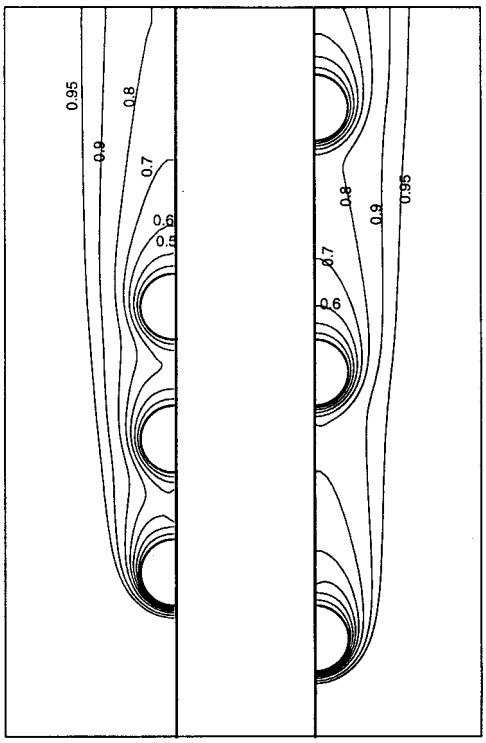

Fig. 4. Dimensionless neutral temperature contours for $l/d = 2$ and 4. $Re = 50$, $Pr = 0.7$, $a/d = 4$, $T_s = 2323$ K, and $T_\infty = 8000$ K. Contours levels shown are, from outermost to inside, 0.95, 0.9, 0.8, 0.7, 0.6, 0.5, 0.4, and 0.3.

comparison with available results by Ramachandran et al. [19] for the three-sphere configuration. The comparison is summarized in Table 1 and shows that the results are in close agreement. As the results for Nusselt number in Ref. [19] did not include gas ionization effects, only the results for the neutral gas flow were compared. To validate the computational model for charged species transport, solutions were obtained with very large inter-particle spacing (8 diameters) at $Re = 50$. The results for the leading sphere were compared with the earlier results of Hader [34] and excellent agreement was observed. The validated code was then used to investigate the effect of inter-particle spacing on flow and transport.

Fig. 3 shows the streamlines for two different longitudinal spacings of 2 and 4 diameters. The lateral spacing is kept constant at $a/d = 4$ with Reynolds number being 50. A distinct evolution of periodicity in flow field is observed after the first particle. At a small longitudinal spacing of 2 diameters, the upstream hemispheres of second and third particles are adversely affected by the wake zones extending from the first and second particles, respectively. In contrast, for higher longitudinal spacing of $l/d = 4$, less significant

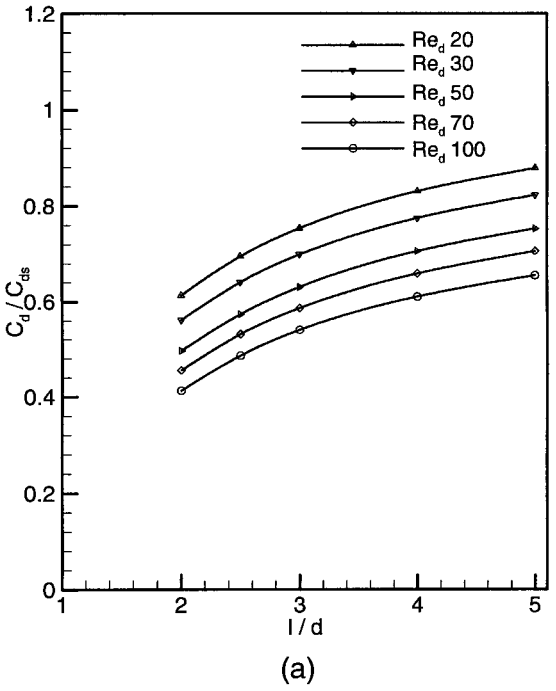

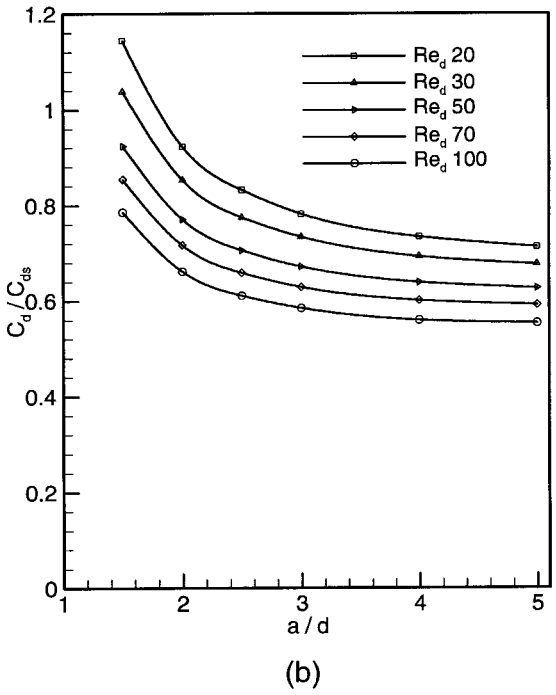

Fig. 5. (a) Variation of the normalized drag coefficient with longitudinal spacing for interior particle at $a/d = 2.5$ and (b) variation of the normalized drag coefficient with lateral spacing for interior particle at $l/d = 4$.

wake interaction is observed between the particles. The neutral temperature contours for the cases considered in Fig. 3 are shown in Fig. 4. For both the cases, the temperature gradients in the front part of the leading sphere are the highest. At small longitudinal spacing, due to the flow stagnation in a region between adjacent spheres, the temperature gradients in the front part of the second and the third particles are much smaller. At large longitudinal spacing, the wake of the upstream particle does not reach the downstream particle. Therefore, with large longitudinal spacing, the temperature gradients in the front part of the trailing spheres are also high. However, even with $l/d = 4$, the temperature contours around the leading particle are not identical to those around the downstream particles.

It is well-established from earlier studies of flow over an array of spheres, that the overall drag coefficient and Nusselt numbers for the second sphere are very close to those for third and the subsequent spheres, provided the longitudinal spacing between colinear spheres is equal. Therefore, the results for the second particle can be considered to reasonably model the behavior of an interior particle of the array. We have presented the results for drag coefficient and Nusselt number such an interior particle. To elucidate the effect of inter-particle interactions, the results are normalized by those for an isolated sphere. The variation of normalized drag coefficient as a function of inter-particle spacing is shown in Fig. 5(a) and (b). In Fig. 5(a), the lateral spacing is kept constant and the longitudinal spacing is varied from $l/d = 2$–5. It is noticed that for all Reynolds numbers, the total drag coefficient increases with increasing longitudinal spacing. For a small longitudinal spacing ($l/d = 2$), the wake zone of the previous particle extends till the upstream hemisphere of the next particle. This creates a low-pressure region in the front, resulting in a reduced pressure drag. Additionally, the recirculating region of the wake causes reversal in the direction of local shear stresses at the upstream hemisphere. This causes a reduction in the friction drag component as well. Therefore, the total drag coefficient decreases with the decrease in longitudinal spacing. Fig. 4(b) shows the variation of the normalized drag coefficient for an interior particle (second particle). The longitudinal spacing is kept constant and the lateral spacing is varied from $a/d = 2$–5. It can be observed that for all Reynolds numbers, the increase in lateral spacing causes a decrease in the normalized drag. This can be attributed to the decrease in surface shear stresses due to the weaker velocity field associated with increased spacing between the lateral neighbors. It causes a reduction in friction drag and, hence, the total-drag coefficient. Additionally, from both the figures, it is observed that for a fixed inter-particle spacing, wake

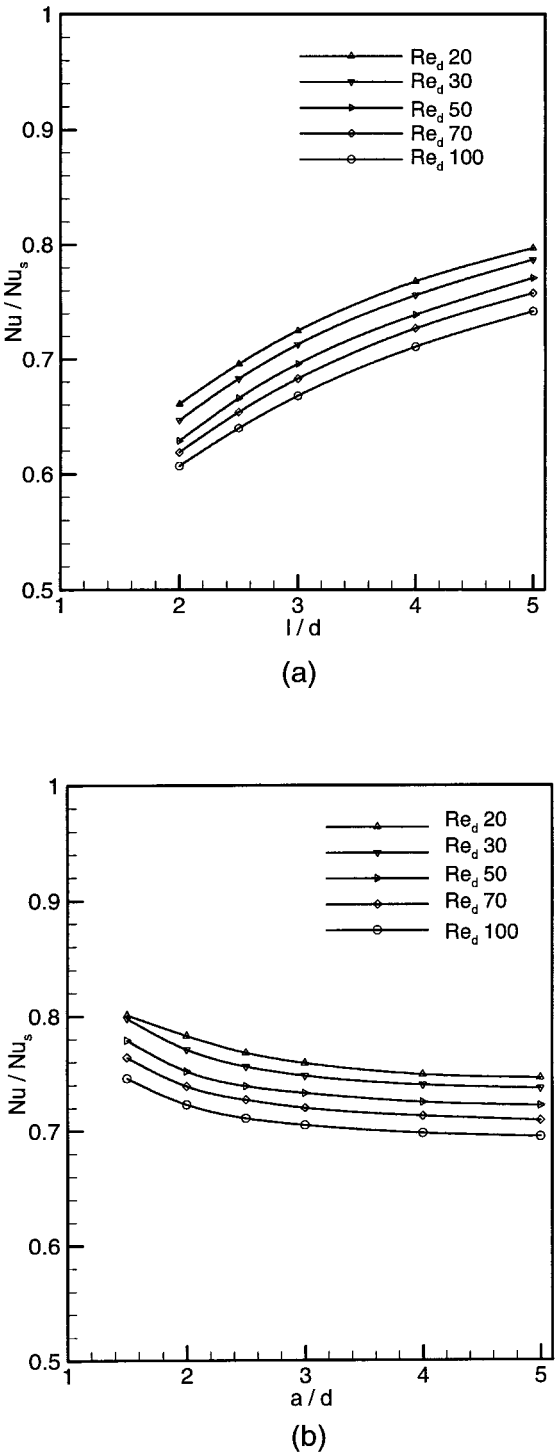

Fig. 6. (a) Variation of the normalized Nusselt number with longitudinal spacing for interior particle at $Pr = 0.7$ and $a/d = 2.5$ and (b) variation of the normalized Nusselt number with lateral spacing for interior particle at $Pr = 0.7$ and $l/d = 4$.

interaction increases with Reynolds number. The numerical results obtained for the normalized drag coefficient for an interior particle for the range of Reynolds number from 20 to 100 with $2 \leq (a/d,\ l/d) \leq 5$ are correlated as

$$\frac{C_d}{C_{ds}} = 1 - (0.86 + 0.006Re^{0.5})(l/d)^{-1.3+0.173\ \ln\ Re} + 5.41Re^{-0.4}\ \exp(-a/d). \quad (18)$$

The above correlation fits the numerical results within a 3% error band. It can be observed that the effect of inter-particle interaction decreases with increasing inter-particle spacing, and the drag coefficient value for an isolated particle is recovered as the lateral and longitudinal spacings become very large.

The results for the variation of normalized overall Nusselt number of an interior sphere with lateral and longitudinal spacing are shown in Fig. 6(a) and (b). Fig. 6(a) shows an increase in overall Nusselt number with increase in longitudinal spacing at all Reynolds numbers. The slope of the curves at $l/d = 5$ suggests that the interaction effect is significant even beyond a longitudinal spacing of 5 diameters. Only when the particle spacing is so large that the cross-stream diffusion can heat the cooler fluid leaving the upstream particle to the temperature of the free stream, each particle will behave as an isolated sphere.

Fig. 6(b) shows a decrease in the overall Nusselt number of the interior sphere with increase in lateral spacing at all Reynolds numbers. This can be attributed to the lowering of velocity field in a region between two lateral neighbors due to an increase in lateral spacing and thus reducing the convective heat transport. The slope of the curves at $a/d = 5$ suggests that the lateral effects diminish beyond a lateral spacing of $a/d = 5$. Additionally, both the figures show a decrease in the normalized overall Nusselt number with increase in Reynolds number for any geometric configuration, thus, indicating the increase in the interaction effect. For instance, at $l/d = a/d = 2.5$, the overall Nusselt number for the interior sphere is about 31–36% less than the isolated sphere for Reynolds number range 20–100, respectively. Using a least square analysis the effect of inter-particle spacing on heat transfer, for the range of Reynolds number from 20 to 100, Prandtl number of 0.7 and $2 \leq (l/d,\ a/d) \leq 5$, is correlated as

$$\frac{Nu}{Nu_s} = 1 - \left(0.571 - \frac{1.08}{Re}\right)(l/d)^{(-0.544+0.0011Re)} + 0.25\ \exp(-a/d). \quad (19)$$

This correlation fits the numerical results within a 3% error band.

5. Conclusions

A steady, laminar axisymmetric thermal plasma flow in an intermediate Reynolds number regime over an array of spherical particles has been analyzed. The effects of longitudinal and lateral spacing on the flow and heat transport have been investigated. The continuum conservation equations for the neutrals and those for ions and electrons have been solved with the Poisson's equation for the self-consistent electric field. A finite volume formulation and a numerically generated orthogonal curvilinear grid have been used. Results show that increasing the longitudinal spacing between particles results in an increase in the drag coefficient and Nusselt number. The influence of the upstream particles is significant even beyond five diameters. Increase in the lateral spacing between the particles causes a decrease in the drag coefficient and Nusselt number. The lateral effects diminish exponentially with increase in spacing. The results for drag and Nuselt number for an interior particle in the array have been found to be substantially different from those for an isolated particle at the same Reynolds number. Correlations that incorporate the effects due to neighboring particles have been proposed for the drag coefficient and the Nusselt number for an interior particle in the array.

Acknowledgements

The support for this work by the National Science Foundation under Grant No. CTS-9733369 is gratefully acknowledged. We also thank Dr M. A. Hader for many stimulating discussions.

References

[1] A. Verdelle, M. Verdelle, P. Fauchais, Influence of velocity and surface temperature of alumina particles on the properties of plasma sprayed coatings, Plasma Chem. Plasma Proc. 2 (1982) 255–291.
[2] Y.P. Chyou, E. Pfender, Behavior of particulates in thermal plasma flow, Plasma Chem. Plasma Proc. 9 (1989) 45–71.
[3] Y.C. Lee, Y.P. Chyou, E. Pfender, Particle dynamics and particle heat and mass transfer in thermal plasmas, Particle Heat and Mass Transfer in Thermal Plasmas 5 (1985) 391–414 Part II.
[4] M.I. Boulos, P. Fauchais, E. Pfender, Thermal Plasmas: Fundamentals and Applications, vol. 1, Plenum Press, New York, 1994.
[5] M.I. Boulos, P. Fauchais, A. Verdelle, E. Pfender, Plasma Spraying: Theory and Application, World Scientific, Singapore, 1993.
[6] R.M. Young, E. Pfender, Nusselt number correlations

for heat transfer to small spheres in thermal plasma flows, Plasma Chem. Plasma Proc. 7 (1987) 211–227.
[7] P. Proulx, J. Mostaghimi, M.I. Boulos, Plasma–particle interaction effects in induction plasma modeling under dense loading conditions, Int. J. Heat Mass Transfer 28 (1985) 1327–1336.
[8] P. Proulx, J. Mostaghimi, M.I. Boulos, Radiative energy transfer in induction plasma modeling, Int. J. Heat Mass Transfer 34 (1991) 2571–2579.
[9] C.T. Crowe, M.P. Sharma, D.E. Stock, The particle-source-in cell (PSI-cell) model for gas-droplet flows, J. Fluids Engng 99 (1977) 325–332.
[10] S.S. Sadhal, P.S. Ayyaswamy, J.N. Chung, Transport Phenomena with Bubbles and Droplets, Springer-Verlag, New York, 1997.
[11] P.S. Ayyaswamy, Direct-contact heat transfer processes with moving liquid droplets, in: J.P. Hartnett, T.F. Irvine, Y.I. Cho (Eds.), Advances in Heat Transfer, vol. 26, Academic Press, New York, 1995, pp. 1–104.
[12] R. Tal, W.A. Sirignano, Cylindrical cell model for the hydrodynamics of particle assemblages at intermediate Reynolds numbers, AIChE Journal 28 (1982) 233–236.
[13] R. Tal, D.N. Lee, W.A. Sirignano, Hydrodynamics and heat transfer in sphere assemblages—cylindrical cell models, Int. J. Heat Mass Transfer 26 (1983) 1265–1273.
[14] S.S. Sripada, P.S. Ayyaswamy, L.J. Huang, Condensation on a spray of water drops: a cell model study—I. Flow description, Int. J. Heat Mass Transfer 39 (1996) 3781–3790.
[15] L.J. Huang, P.S. Ayyaswamy, S.S. Sripada, Condensation on a spray of water drops: a cell model study—II. Transport quantities, Int. J. Heat Mass Transfer 39 (1996) 3791–3797.
[16] S.J. Chen, A.Y. Tong, Application of elliptic grid generation technique to the solution of hydrodynamics and heat transfer of droplet arrays at intermediate Reynolds numbers, Int. J. Heat Mass Transfer 31 (1988) 1063–1072.
[17] J.S. Tsai, A.M. Sterling, The application of an embedded grid to the solution of heat and momentum transfer for spheres in a linear array, Int. J. Heat Mass Transfer 33 (1990) 2491–2502.
[18] R.S. Ramachandran, T.Y. Wang, C. Kleinstreuer, H. Chiang, Laminar flow past three closely spaced monodisperse spheres or non-evaporating drops, AIAA Journal 29 (1991) 43–51.
[19] R.S. Ramachandran, C. Kleinstreuer, T.Y. Wang, Forced convection heat transfer of interacting spheres, Numerical Heat Transfer, Part A 15 (1989) 471–489.
[20] P.M. Chung, L. Talbot, K.J. Touryan, Electric Probes in Stationary and Flowing Plasmas: Theory and Application, Springer-Verlag, New York, 1975.
[21] M.A. Jog, Analysis of heat transfer to a spherical particle from continuum plasma, J. Appl. Phys. 78 (1995) 1424–1429.
[22] M.A. Jog, L. Huang, Transient heating and melting of particles in plasma spray coating process, J. Heat Transfer 118 (1996) 471–477.
[23] S.S. Sripada, I.M. Cohen, P.S. Ayyaswamy, A study of the EFO discharge process used for ball bonding in Microelectronic Packaging. New York, ASME HTD-336 (1996) 129–136.
[24] M.A. Jog, I.M. Cohen, P.S. Ayyaswamy, Electrode heating in a wire-to-plane arc, Physics of Fluids B4 (1992) 465–472.
[25] M.A. Hader, M.A. Jog, Continuum plasma flow past a sphere, Physics of Plasmas 5 (1998) 902–909.
[26] Eca, 2D Orthogonal grid generation with boundary point distribution control, J. Comp. Physics 125 (1996) 440–453.
[27] J.R. Fincke, W.D. Swank, C.L. Jeffery, Simultaneous measurement of particle size, velocity, and temperature in thermal plasma, IEEE Trans. Plasma Sci. 18 (1990) 948–957.
[28] E. Bourdin, P. Fauchais, M.I. Boulos, Transient heat conduction under plasma conditions, Int. J. Heat Mass Transfer 26 (1983) 567–582.
[29] M. Mitchner, C.H. Kruger, Partially Ionized Gases, Wiley, New York, 1962.
[30] E. Hinnov, J.G. Hirshberg, Electron–ion recombination in dense plasmas, Physical Review 125 (1962) 795–801.
[31] S.V. Patankar, Numerical Heat Transfer and Fluid Flow, McGraw-Hill, New York, 1980.
[32] A. Verma, Analysis of heat transfer to an array of particles in plasma spray coating process, M.S. Thesis, University of Cincinnati, 1998.
[33] S.C. Brown, Basic Data of Plasma Physics, MIT Press, Cambridge, 1967.
[34] M.A. Hader Heat transfer to a particle from a thermal plasma. Ph.D. Thesis, University of Cincinnati, 1998.